High Integrity Localization of Intelligent Vehicles with Student's t Filtering and Fault Exclusion

Joelle Al Hage, Nicolò Salvatico, Philippe Bonnifait

High Integrity Localization of Intelligent Vehicles with Student's t Filtering and Fault Exclusion

Joelle Al Hage, Nicolò Salvatico and Philippe Bonnifait

***Abstract*—High-integrity localization is a key element for safety-critical applications like autonomous driving. The navigation filter plays a crucial role in merging sensor data to estimate an accurate pose and calculate a confidence interval based on task requirements. This paper presents an end-to-end Student's t information filter for accurate data fusion and non-pessimistic confidence domain computation. The filter incorporates a Fault Detection and Exclusion stage based on the Kullback-Leibler Divergence. The degree of freedom of the t distribution shapes the heavy tail to make the estimation process more robust against non detected outliers. We show that the adjustment of the degree of freedom can be done in real time using measurement residuals which give an indirect vision of the environment complexity. The accuracy and integrity of the proposed approach are evaluated with real data acquired with an experimental vehicle using GPS and Galileo pseudoranges merged with camera measurements after a map matching step with a High-Definition map. A comparative study with other classical methods based on Kalman filtering is also reported.**

I. Introduction

Localization with high integrity is a major challenge for safe navigation of intelligent vehicles. This requires the localization system to issue a safety alert when it should not be used. Vehicle localization on roads relies on the fusion of data collected from multiple sensors, including Inertial Measurement Unit (IMU), Global Navigation Satellite Systems (GNSS), cameras, and Lidars [1]. Furthermore, the incorporation of a High-Definition (HD) map is crucial to associate perception measurements with georeferenced features [2]–[4].

Merging data from multiple sensors is usually done using a Kalman Filter (KF). However, the assumption of Gaussian distributions is not always justified and can be problematic when bounding the errors under small probabilities. This principle is linked to the integrity concept.

The integrity of intelligent vehicles, that originates from the aviation domain, is today an active research area that aims to reduce the probability of accidents as much as possible [5], [6]. It refers to the trust that can be placed in a navigation solution and is associated with a target integrity risk (TIR) that represents the maximum probability that the error in position exceeds a limit without warning the user [5], [7]. The error bound (or confidence interval) is known as the Protection Level (PL) and is computed so that the probability of the position error exceeding it is less than the TIR.

In this paper, the aim is to achieve a high integrity localization while maintaining a lane-level accuracy. The PL values must be determined in real time without an underestimation due to biases, non Gaussian distributions or errors resulting from the linearization of models. The Student's t filter (StF) which is a generalization of the KF is well suited to these problems since it handles heavy tailed distributions [8]. Multiple adaptation of this filter can be found in the literature [9]–[12].

The heavy tail property is important to bound the errors in challenging environments. In this paper, an end-to-end approach based on Bayesian Student's t filtering is proposed for data fusion and simultaneous PL computation. Pseudoranges from different GNSS constellations and measurements from a smart camera are modeled as Student's t distribution and are merged with odometery data through a Tightly Coupled (TC) architecture [13]. The integration of low-level GNSS measurements in data fusion allows for improved modeling, resulting in superior integrity performance compared to a loosely coupled scheme that relies on the position solution provided by a GNSS receiver. Although the StF is more robust than KF, large errors still affect the localization accuracy and integrity. Therefore, a Fault Detection and Exclusion (FDE) based on the Kullback-Leibler Divergence (KLD) is proposed to remove the erroneous measurements from the data fusion. The Student's t Information Filter (StIF), proposed in our previous work, is used to simplify the fault exclusion [14]. Mathematically equivalent to the StF, the key aspect of the StIF lies in its update step, which is modeled as a summation of the information contributions. Unlike [14], in this paper, raw measurements are modeled as Student's t distributions to improve the integrity performance.

The StF is based on t-distributions characterized by a Degree of Freedom (DoF) which influences the tails to be lighter or heavier. When the DoF approaches infinity, the t-distribution becomes similar to a Gaussian. The DoF has a large influence on the filter and on the confidence interval values. An incorrect setting can lead to suboptimal behavior. In certain studies such as [8], a choice is made to set the DoF equal to three to preserve heavy tails. However, this particular choice is not suitable for our application, considering the dynamic nature of the environment. For instance, opting for this value in an open sky environment can lead to a degradation of the filter results. In [10], the authors deal with this problem through a robust Multiple Model Adaptive Estimation (MMAE) where a bank of three StF with different DoF values is used. The MMAE selects the best filter or combine the outputs of the different StF. This method limits the number of possible choices on the DoF. In this paper, we propose to adapt the DoF accordingly to the residual computed for the fault detection. This residual

The authors are with Heudiasyc laboratory, UMR 7253 CNRS, Université de Technologie de Compiègne, France. This work is part of the ANR ToICar project (ANR-21-CE33-0012) and the SIVALab joint laboratory.

includes information about the quality of pseudoranges and camera measurements.

This paper is organized as follows: section II presents the proposed multi-sensor data fusion through a tightly coupled architecture using the student's t information filter. Section III presents the fault detection and exclusion step based on the KLD and the integrity study. Experimental results and discussions based on real data are given in section IV.

II. Multi-sensor data Fusion using GNSS pseudoranges and camera measurements

A. System modeling

Let's consider a vehicle equipped with wheel-speed sensors, a yaw-rate gyro, a GNSS receiver and a smart camera for lane marking detection. The localization problem is defined as estimating the vehicle pose with respect to a local ENU (East-North-Up) frame (R_O in figure 1). The vehicle pose is defined at the body frame located at the middle of the rear axis (R_B). For a tightly coupled data fusion scheme, the state vector at epoch k is defined as:

$$X_k = [x, y, z, \theta, cdt, c\dot{dt}]_k^T. \tag{1}$$

The receiver clock offset cdt (multiplied by the speed of light c) and clock drift $c\dot{dt}$ with respect to GPS time are part of the state vector and are estimated within the filter, along with the pose (θ is the heading). When dealing with two constellations, e.g. GPS and Galileo, to avoid adding variables to the state vector that represent receiver clock bias and drift with respect to Galileo system time, the estimate of the Galileo to GPS Time Offset (GGTO) can be used [15].

The evolution model involves odometric data as input:

$$X_{k+1} = f(X_k, u_k) + v_k, \tag{2}$$

where $u_k = [\Delta_k, \Omega_k]$ is composed of the elementary displacement and rotation obtained from the wheel-speed sensors and the gyro respectively. The process noise v_k is modeled as a Student's t distribution with zero mean, DoF γ and scale matrix Q:

$$v_k \sim St(0, Q_k, \gamma_k). \tag{3}$$

If a Gaussian distribution is sufficient for modeling v_k, a high value of γ that tends to infinity can be chosen.

Consider m pseudoranges acquired at epoch k, the corrected pseudorange ρ_j can be written as:

$$\rho_j = R_j + cdt + \epsilon, \tag{4}$$

where R_j is the Euclidean distance between the receiver and satellite j and ϵ is the receiver noise.

As pseudoranges link the satellites to the receiver antenna located at the roof of the vehicle (R_G), the transformation between the antenna and the body frame is used:

$$\begin{bmatrix} x \\ y \\ z \end{bmatrix} = \begin{bmatrix} x \\ y \\ z \end{bmatrix}_{GNSS} - \begin{bmatrix} \cos\theta & -\sin\theta & 0 \\ \sin\theta & \cos\theta & 0 \\ 0 & 0 & 1 \end{bmatrix} \begin{bmatrix} t_x \\ t_y \\ t_z \end{bmatrix}. \tag{5}$$

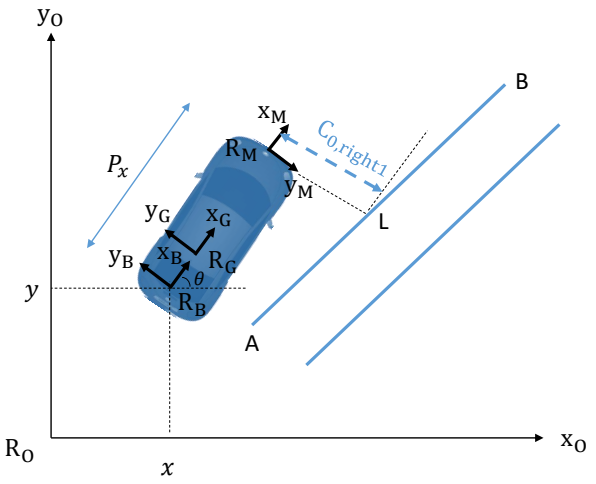

Fig. 1: Frames. The camera detects a geo-referenced lane marking [AB] on the right.

The Euclidean distance is written as:

$$R_j = \sqrt{\begin{array}{c}(x + t_x\cos\theta - t_y\sin\theta - x_j)^2 + \\ (y + t_x\sin\theta + t_y\cos\theta - y_j)^2 + (z + t_z - z_j)^2\end{array}} \tag{6}$$

where (x_j, y_j, z_j) are the coordinates of satellites j in the ENU frame, $(x, y, z)_{GNSS}$ corresponds to the antenna position and (t_x, t_y, t_z) is the translation of the antenna with respect to the body frame.

Given equation 4, the model of ρ is expressed as:

$$Z_k = h_k(X_k) + \omega_k, \tag{7}$$

where ω_k is the noise associated to the pseudorange measurements modeled as a Student's t distribution with zero mean, DoF δ and scale matrix R:

$$\omega_k \sim St(0, R_k, \delta_k). \tag{8}$$

We take advantage of this modeling to improve the integrity of the state estimation. The details will be shown in the next section.

Beside GNSS measurements, another observation model is used for lane measurements from a smart camera. The camera used is able to detect up to four lane markings at a time (two at each side) and return lateral distances denoted C_0 (figure 1). C_0 refers to the signed distance between R_M and the intersecting point L at the map-matched segment [AB] of the HD map. The camera observation is expressed as [16]:

$$C_0 = \frac{(P_x\sin\theta + y - y_A)x_{AB} - (P_x\cos\theta + x - x_A)y_{AB}}{x_{AB}\cos\theta + y_{AB}\sin\theta}. \tag{9}$$

P_x is the distance between R_B and R_M. For more details, the reader can refer to [7]. As in the case of GNSS, the noise ω_k associated to the camera measurements is modeled as a Student's t distribution to improve the integrity in presence of poor perception data.

Given these models, the state filtering is presented in the following.

B. State filtering

Let X be a random variable that follows a multivariate Student's t distribution: $X \sim St(\mu, P, \nu)$ where μ is the mean vector, P is the scale matrix and ν is the degree of freedom (DoF) [17]. The covariance is defined when $\nu > 2$ and is linked to the scale matrix by $\Sigma = \frac{\nu}{\nu-2}P$.

The development of Student's t filters is more challenging than Kalman filters, as careful approximations must be taken into account to avoid undesired behaviors [8]. In this paper, the informational form of the Student's t filter (StIF) developed in [14] is used. The StIF is equivalent to the StF but its advantage appears in the update step thanks to the summation of the information contributions that make it suitable for multi-sensor data fusion and for fault detection and exclusion.

The distribution of noises are described as Student's t distributions as given in equations 3 and 8. The initial state is also described as a t distribution: $St(X_0, P_0, \nu_0)$ where X_0, P_0 and ν_0 are the initial guesses.

Compared to the StF, the StIF features an information matrix (up to a constant) and an information vector computed from the scale matrix and the state vector as [14]:

$$Y_k = P_k^{-1}, \tag{10}$$

$$y_k = Y_k X_k. \tag{11}$$

These equations are obtained in a similar manner to the informational form of the KF, known as the Information Filter (IF) [18].

The StIF includes two steps: time update and measurement update.

At time k, suppose that $p(X_k|Z_{1:k})$ follows a t distribution $St(X_{k|k}, P_{k|k}, \nu_k)$ and $p(v_k)$ is given in equation 3. To derive the prediction step of the StIF, these two distributions must share a common DoF denoted ν'_k [8], [19]. In order to preserve the heaviest tail between the two distributions, ν'_k may be chosen as [19]:

$$\nu'_k = \min(\nu_k, \gamma_k). \tag{12}$$

In our case, the heavy tail property is important to ensure the integrity of the state estimation.

Given this new DoF, the scale matrices $P_{k|k}$ and Q_k must be adjusted in $P'_{k|k}$ and Q'_k. This can be obtained by moment matching or by minimizing the Kullback-Leibler divergence [19]. In this work, the matrix adjustment is done by minimizing a modified upper bound of the KLD as proposed in [11].

Using a first-order Taylor approximation and given that linear transformations preserve the DoF of a Student's t distribution [17], the predicted distribution can be approximated as:

$$p(X_{k+1}|Z_{1:k}) \sim St(X_{k+1|k}, P_{k+1|k}, \nu'_k), \tag{13}$$

where

$$X_{k+1|k} = f(X_{k|k}, u_k), \tag{14}$$

$$P_{k+1|k} = F_k P'_{k|k} F_k^T + Q'_k. \tag{15}$$

which can be written in the informational form:

$$Y_{k+1|k} = P_{k+1|k}^{-1}, \tag{16}$$

$$y_{k+1|k} = Y_{k+1|k} X_{k+1|k}, \tag{17}$$

where F_k is the Jacobian matrix.

Likewise, to derive the measurement update, a choice on the DoF must be made. Keeping the same policy as in the prediction step, ν''_k may be chosen as:

$$\nu''_k = \min(\nu'_{k-1}, \delta_k). \tag{18}$$

Then:

$$p(X_k, w_k|Z_{1:k-1}) = St\left(\begin{bmatrix} X_{k|k-1} \\ 0 \end{bmatrix}, \begin{bmatrix} P'_{k|k-1} & 0 \\ 0 & R'_k \end{bmatrix}, {\nu''}_k\right) \tag{19}$$

where $P'_{k|k-1}$ and R'_k are the adjusted matrices of $P_{k|k-1}$ and R_k given ν''_k.

The posterior distribution $p(X_k|Z_{1:k})$ is then expressed as a Student's t distribution $St(X_{k|k}, P_{k|k}, \nu_k)$ and the updated parameters in the informational form are given by [8], [10], [14]:

$$\nu_k = \nu''_k + d_Z, \tag{20}$$

$$Y_{k|k} = c_k^{-1}(Y_{k|k-1} + \sum_{i=1}^{N} I_{i,k}), \tag{21}$$

$$y_{k|k} = c_k^{-1}(y_{k|k-1} + \sum_{i=1}^{N} i_{i,k}), \tag{22}$$

$$c_k = \frac{\nu''_k + \Delta_k^2}{\nu''_k + d_Z}, \tag{23}$$

where d_Z is the dimension of the observation vector, N is the number of observations assumed to be uncorrelated with each other, $\Delta_k^2 = (Z_k - h(X_{k|k-1}))^T S_k^{-1}(Z_k - h(X_{k|k-1}))$ is the Mahalanobis distance and $S_k = H_k P_{k|k-1} H_k^T + R_k$ is the innovation scale matrix.
$I_{i,k} = H_{i,k}^T R_{i,k}^{-1} H_{i,k}$ and $i_{i,k} = H_{i,k}^T R_{i,k}^{-1} Z_{i,k}$ are the information contributions of the observation $Z_{i,k}$. Since the observation model is non linear, $i_{i,k}$ is expressed as:

$$i_{i,k} = H_{i,k}^T R_{i,k}^{-1}[Z_{i,k} - h_i(X_{k|k-1}) + H_{i,k} X_{k|k-1}],$$

where $H_{i,k} = \frac{\partial h_i}{\partial X}|_{X=X_{k|k-1}}$ is the Jacobian matrix corresponding to the measurement model Z_i (pseudorange or camera measurements).

The updated equations are similar to the IF, but scaled by a term c_k that depends on the Mahalanobis distance between the measurement and its prediction. Therefore, it enables the filter to be aware of the observation quality and to scale the overall measurement update. Hence, if the measurement differs significantly from its prediction, an increase in the covariance matrix appears.

From equation 20 and after the first update step, the DoF increases to ν_k. Without the limitation applied in the prediction step (equation 12), the DoF would tend to infinity and the

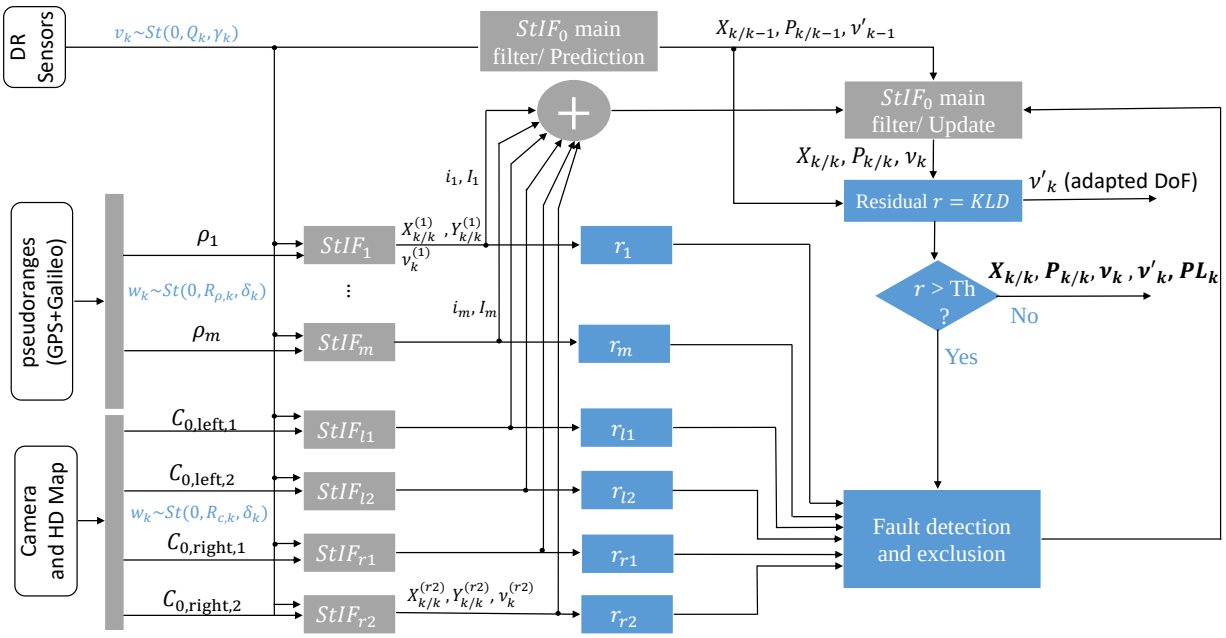

Fig. 2: General architecture of the proposed method. v and w are the process and measurements noises respectively, ν the DoF, X the state vector and P the scale matrix. C_0 the measurements from the camera. St for Student's t.

StIF would converge to an IF. Regarding the initial values of γ, δ and ν'_0, they are assumed to be equal and this choice is maintained over time. Therefore, ν''_k is equal to ν'_{k-1} (equation 18) and no approximation is needed when going from time update to measurement update. However, a bad value of the DoF affects the accuracy and integrity of the estimate. In order to avoid setting a fixed DoF, especially when the environment changes, a strategy to define it is presented in the next section by taking advantage of the FDE step.

III. High integrity for multi-sensor data fusion

A. Fault detection and exclusion

Although the StIF is designed to be more robust than the IF in the presence of faults, the latter still influence the quality of the filter estimates. For this purpose a fault detection and exclusion able to exclude faulty measurements is proposed.

The generation of a residual is the first step of an FDE where the KLD between the updated and the predicted distributions is used. As discussed before, the predicted distribution $p(X_k|Z_{1:k-1})$ follows a t distribution with mean $X_{k|k-1}$, DoF ν'_{k-1} and scale matrix $P_{k|k-1}$ (equation 15). The updated distribution $p(X_k|Z_{1:k})$ follows a t distribution with mean $X_{k|k}$, DoF ν_k and scale matrix $P_{k|k}$ (inverse of equation 21).

To simplify the equation of the KLD, we propose to approximate the original distributions by Gaussian distributions. Let q_1 and q_2 be the approximated Gaussian distributions of the predicted and updated distributions, respectively. $X_{k|k-1}$ and $\frac{\nu'_{k-1}}{\nu'_{k-1}-2}P_{k|k-1}$ are the mean and covariance of q_1. Likewise, $X_{k|k}$ and $\frac{\nu_k}{\nu_k-2}P_{k|k}$ are the mean and covariance of q_2. This approximation is sufficient for residual computation.

Given these covariance matrices, the corresponding information matrices are:

$$Y_{\Sigma,k|k-1} = (\frac{\nu'_{k-1}}{\nu'_{k-1}-2}P_{k|k-1})^{-1}, \tag{24}$$

$$Y_{\Sigma,k|k} = (\frac{\nu_k}{\nu_k-2}P_{k|k})^{-1}. \tag{25}$$

The residual r_k is defined as the KLD of the predicted distribution q_1 from the updated distribution q_2 ($KLD(q_2||q_1)$) and is given by [20]:

$$\begin{aligned} r_k = \frac{1}{2}[&(X_{k|k}-X_{k|k-1})^T Y_{\Sigma,k|k-1}(X_{k|k}-X_{k|k-1}) \\ &+ trace(Y_{\Sigma,k|k-1}Y^{-1}_{\Sigma,k|k}) + \log\frac{|Y_{\Sigma,k|k}|}{|Y_{\Sigma,k|k-1}|} - d], \end{aligned} \tag{26}$$

where d is the dimension of the state vector. For this computation, only $[x, y, z, \theta]$ are used, then $d = 4$.

The residual given in equation 26 acts in the state space and takes into account two types of information: the Burg matrix divergence and the Mahalanobis distance [21]. Using this residual, we are not interested by detecting a fault that has no direct effect on the pose estimation. Likewise, two types of tests are taken into account: test on the mean and test on the covariance matrices.

It should be noted that the KLD is computed with respect to the updated distribution because the StIF increases the covariance in the presence of fault. Therefore, the information

lost when the prediction is used to approximate the update is more important than the opposite case.

Once the residual r_k for the current epoch is generated with a filter (called main filter) that uses all available observations, it must be compared to a threshold Th in order to complete the detection phase. The residual follows a distribution related to Chi-squared and F-distributions as in [21]. The threshold is then set according to a false alarm probability. If $r_k > Th$, faults are detected and must be isolated before delivering the state estimate. For this purpose, a bank of filters is generated wherein every StIF does the measurement update using only one observation Z_j (camera or GNSS pseudorange):

$$Y_{j,k|k} = c_{j,k}^{-1}(Y_{k|k-1} + I_{j,k}), \tag{27}$$

$$y_{j,k|k} = c_{j,k}^{-1}(Y_{k|k-1} + i_{j,k}), \tag{28}$$

$$X_{j,k|k} = Y_{j,k|k}^{-1} y_{j,k|k}. \tag{29}$$

The residual $r_{j,k}$ associated to each observation is then computed in a comparable manner to equation 26.

Once these computations are performed, the maximum residual r_j is found and is compared to the corresponding threshold Th_j (the false alarm is not necessarily the same for each type of sensor). If the residual exceeds the threshold, the considered observation is excluded from the main filter. After the fault exclusion, the filter estimate is computed again and the FDE is repeated until no more faults are detected using the main filter (figure 2).

Concerning the StIF, measurement Z_j is excluded from the fusion procedure by subtracting its information contribution ($I_{j,k}$, $i_{j,k}$) from the main filter and by updating the c term.

After the FDE step, the fixed DoF given in equation 12 is replaced by an adaptive DoF that changes according to the residual values. Indeed, the residual provides an indication about the environment and the quality of the measurements. When this residual is large, measurements are likely to be noisy and tails should be heavier, so the DoF has to decrease. However, for small residual values, a lighter tail may be reasonable, so the DoF increases. Therefore, the adaptation of the DoF makes use of the residual computed by the fault detection phase, according to a negative exponential model with a minimum value:

$$\begin{cases} \nu'_k = a.\exp(b.r_k) & r_k < l \\ \nu'_k = 3 & r_k > l \end{cases} \tag{30}$$

where a, b and l are tuning parameters. For numerical stability and to be able to compute a covariance matrix, the minimum allowed DoF is chosen equal to 3.

The general architecture of the method is given in figure 2.

B. Protection level computation

One of the objectives of using Student's t modeling is to bound in real-time the estimation errors without underestimating the PL bound. When dealing with localization integrity, a PL must be able to handle small target integrity risk (e.g. $TIR = \alpha \leq 10^{-3}$). The heavy tail property is fundamental for such a computation. So far, there is no consensus about the TIR value which should depend on the level of autonomy and operational design domain. To bound the errors, the matrix $P_{k|k}$ obtained in the measurement update is adjusted to $P'_{k|k}$ according to the minimum between ν'_k (equation 30) and ν_k (equation 20):

$$N_1 = \min(\nu_k, \nu'_k). \tag{31}$$

Note that if the minimum corresponds to ν_k, no adaptation is needed. The PL is then expressed as [22]:

$$PL(\alpha) = K(\alpha, N_1)\sqrt{N_1 \times \max\left(\text{eigenvalue}(P'_{k|k})\right)}, \tag{32}$$

where $K(\alpha, N_1)$ is obtained from a multivariate t distribution with DoF N_1 and according to the confidence level α [7].

IV. Experimental results and discussions

In this section, the approach is evaluated on data acquired with an experimental vehicle equipped with a Septentrio AsteRx SB PRO Connect for Galileo and GPS pseudorange measurements, wheel-speed sensors, a yaw-rate gyro, a Mobileye camera for lane marking detection, a NovAtel SPAN CPT for the ground truth and an HD map. Acquisitions were made at a frequency of 50Hz for dead-reckoning, 35Hz for the camera (sub-sampled at 3.5Hz to reduce time correlation) and 1Hz for GNSS measurements. The state estimation is computed at 50Hz.

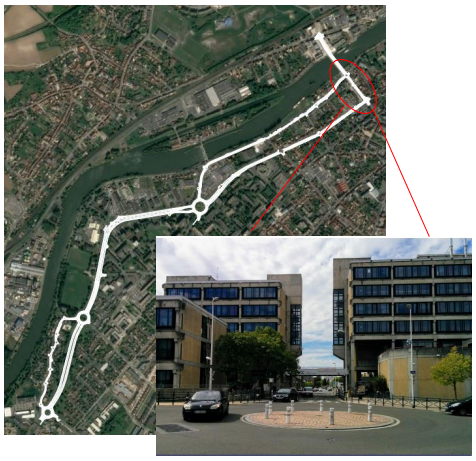

Fig. 3: Compiègne suburban test and university campus.

The vehicle was driven within the town of Compiègne for about 6 km in a suburban (to urban) area with some challenging GNSS parts as shown in figure 3. During the acquisition, the lane markings were not of high quality and mostly the roadsides were detected instead.

The error in the Along Track (AT) and Cross Track (CT) directions for the StIF before and after the FDE step are shown in figure 4. For more details about the computation of these errors, the reader can refer to [7]. It can be noticed the improvement brought by the FDE step to the localization accuracy. Regarding the FDE, the residual used for the fault detection is shown in figure 5 with the associated threshold. The residuals used for the camera fault exclusion are shown in

figure 6. The camera measurements give rise to multiple issues that can arise from incorrect measurement association with the HD map, poor marking quality, or faulty measurements. As for the GNSS pseudoranges, the number of excluded measurements is more limited. For instance, at the start of the trajectory, the low elevated satellite G17 is excluded (figure 7). Similarly, around the university campus (near sample 1.8×10^4), several satellites, such as E25 and G32 , from Galileo and GPS constellations respectively, are excluded due to the harsh environment and their low elevations.

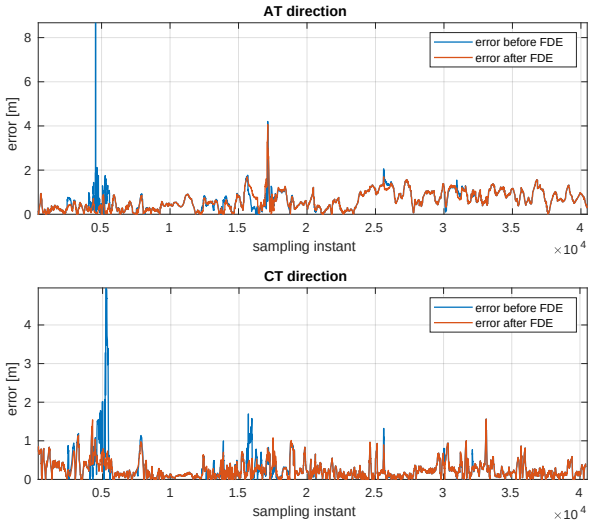

Fig. 4: Errors before (in blue) and after (in red) the FDE step.

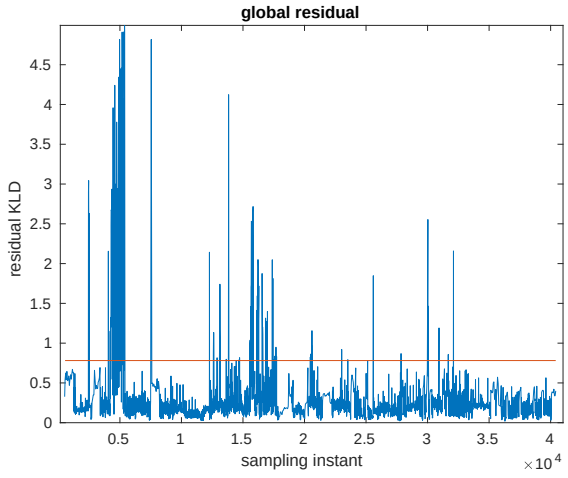

Fig. 5: Residual for fault detection in blue, threshold in red.

Figure 8 illustrates the adaptive DoF computed by the filter. The parameters for equation 30 are set as $a = 20.114, b = -0.0791$ and $l = 40$. To preserve heavy tails, which contribute

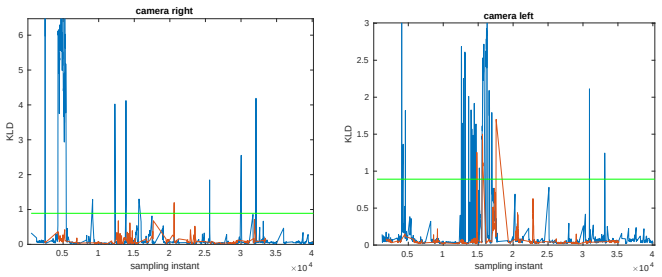

(a) Right side (b) Left side

Fig. 6: Camera residuals in the left and right sides (first measurement in blue, second in red). Threshold in green.

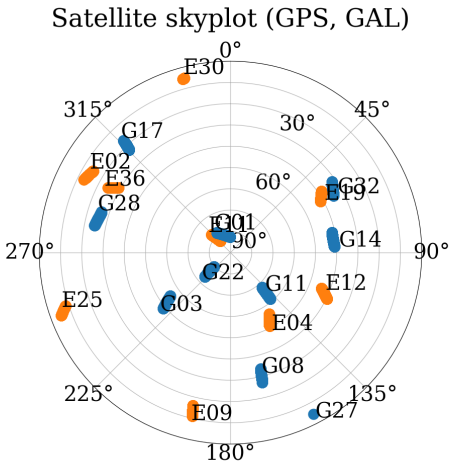

Fig. 7: GPS (G) and Galileo (E) elevations.

to the enhancement of the filter's integrity, an upper bound of 20 is imposed on the DoF.

Table I presents the performance evaluation of the StIF in terms of accuracy and integrity, along with a comparison to an extended information filter (EIF). The results are provided for both cases, with and without camera fusion, while always incorporating the fusion of pseudorange measurements. The proposed StIF and EIF exhibit comparable accuracy performance. In terms of consistency and computed integrity risk, the StIF demonstrates superior performance for a TIR of 10^{-3}. Without the FDE step and camera fusion, the StIF ensures integrity in the CT direction, while the EIF fails. After integrating camera measurements, both filters fail to meet the integrity requirement before the FDE step ($P(error > PL) = IR > 10^{-3}$). However, the StIF shows significantly better values. After the FDE step, the StIF verifies the integrity requirement in the CT direction, while the EIF does not. The importance of the FDE step for integrity and accuracy can be highlighted.

It should be noted that the improved integrity of the StIF compared to the EIF should not come at the expense of an increased uncertainty values that could diminish the availabil-

	Without FDE				With FDE based on the KLD				
	GNSS		GNSS-camera		GNSS		GNSS-camera		
	StIF	EIF	StIF	EIF	StIF	EIF	StIF	EIF	DoF=3
absolute AT error [m]	0.69	0.68	0.63	0.62	0.68	0.68	0.61	0.6	0.78
absolute CT error [m]	0.68	0.67	0.28	0.28	0.61	0.66	0.24	0.27	0.24
mean absolute error [m]	1.07	**1.05**	0.76	**0.74**	**1**	1.04	**0.71**	0.72	0.86
$IR_{AT} \times 10^{-3}$	**1.3**	1.6	**1.1**	3.9	**1.3**	1.6	1.5	1.8	**0.02**
$IR_{CT} \times 10^{-3}$	**0**	10	**6.8**	22	**0**	10	0.9	15	**0**

TABLE I: Errors and computed integrity risk (IR) (per sample) for EIF and StIF in the AT and CT directions ($TIR = 10^{-3}$). "StIF" refers to the proposed filter with adaptive DoF. "DoF=3" refers to StIF with fixed DoF.
The best values are in bold. In dark blue, the integrity requirement is verified.

ity of autonomous systems. Figure 9 shows the calculated PL in the AT and CT directions (TIR of 10^{-3}). Results are presented for the StIF with adapted DoF and the EIF, with camera fusion and FDE step. The StIF, while ameliorating integrity compared to the EIF, provides non-pessimistic PL with a mean values of 2.1m in the AT direction and 1.2m in the CT direction. These value are close to that of the EIF. The StIF has the advantage of increasing PL values in challenging areas. The results of a StIF with a fixed DoF=3 are also presented in table I and figure 9. This filter guarantees integrity in the AT and CT directions at the expense of reduced accuracy and increased PL values. In this case, the PL mean values are approximately 5.7m in the AT direction and 4.1m in the CT direction which shows that this filter is much more pessimistic.

The camera demonstrates a notable impact on reducing errors and PL in the CT direction. However, as this sensor is not use to detect markings in the AT direction, it does not have a great effect in that particular direction.

Based on the obtained results, it can be concluded that the end-to-end StIF with adaptive DoF is a promising approach for consistent multi-sensor data fusion using raw data. However, several points must be taken into account. Firstly, the parameters for the adaptive DoF must be carefully tuned as they have a significant impact on the performance of the filter. In our case, these values are selected based on the desired relationship between the residual and DoF. Likewise, the tuning of scale matrices of the measurements and process noises presents a similar challenge. These values are determined based on the covariances tuned for the Gaussian filter (EIF). These tuning processes require certain expertise and domain knowledge.

V. Conclusion

An end-to-end Student's t filter with adaptive DoF for data fusion and PL computation was proposed. To enhance localization accuracy and integrity, an FDE was added to exclude outliers. This step uses residuals based on the Kullback-Leibler divergence. The DoF is dynamically adjusted based on the quality of the observations. Experimental results demonstrate the superiority of the proposed method in achieving consistent and accurate localization using raw sensors data. Notably, the proposed method outperforms the traditional KF while maintaining non pessimistic uncertainty values.

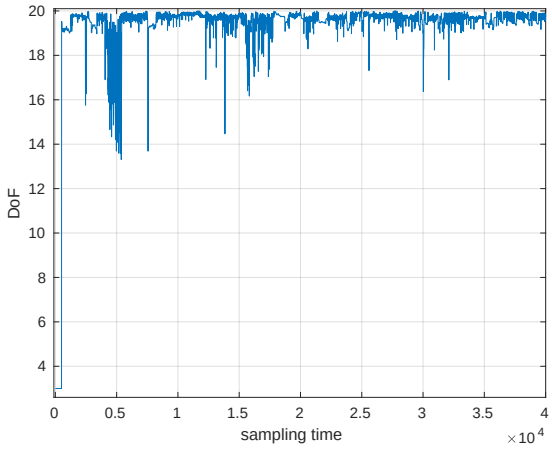

Fig. 8: Adaptation of the DoF.

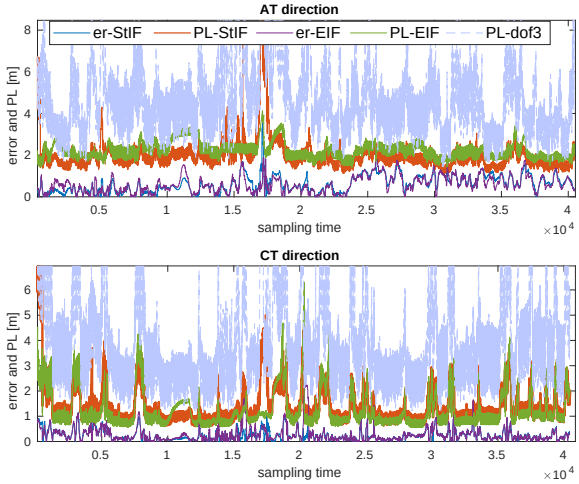

Fig. 9: Errors and PLs for the StIF with adapted DoF and for the EIF. PLs for the StIF with DoF=3.

In future research, the scale matrices of measurements and process noises will be determined through a data driven approach. Additionally, the impact of non-linearity and its influence on the filter will be addressed.

REFERENCES

[1] S. Li, X. Li, H. Wang, Y. Zhou, and Z. Shen, "Multi-gnss ppp/ins/vision/lidar tightly integrated system for precise navigation in urban environments," *Information Fusion*, vol. 90, pp. 218–232, 2023.

[2] M. A. Quddus, W. Y. Ochieng, and R. B. Noland, "Current map-matching algorithms for transport applications: State-of-the art and future research directions," *Transportation Research Part C: Emerging Technologies*, vol. 15, no. 5, pp. 312–328, Oct. 1, 2007.

[3] A. Kasmi, J. Laconte, R. Aufrère, R. Theodose, D. Denis, and R. Chapuis, "An information driven approach for ego-lane detection using lidar and openstreetmap," in *16th International Conference on Control, Automation, Robotics and Vision*, 2020, pp. 522–528.

[4] F. Ghallabi, M.-A. Mittet, E.-H.-S. Ghayath, and F. Nashashibi, "Lidar-based high reflective landmarks for vehicle localization in an hd map," in *2019 IEEE Intelligent Transportation Systems Conference (ITSC)*, 2019, pp. 4412–4418.

[5] N. Zhu, J. Marais, D. Bétaille, and M. Berbineau, "GNSS position integrity in urban environments: A review of literature," *IEEE Transactions on Intelligent Transportation Systems*, vol. 19, no. 9, pp. 2762–2778, 2018.

[6] D. Margaria and E. Falletti, "The local integrity approach for urban contexts: Definition and vehicular experimental assessment," *Sensors*, vol. 16, no. 2, p. 154, 2016.

[7] J. Al Hage, P. Xu, P. Bonnifait, and J. Ibanez-Guzman, "Localization integrity for intelligent vehicles through fault detection and position error characterization," *IEEE Transactions on Intelligent Transportation Systems*, vol. 23, no. 4, pp. 2978–2990, 2022.

[8] M. Roth, E. Özkan, and F. Gustafsson, "A student's t filter for heavy tailed process and measurement noise," in *International Conference on Acoustics, Speech and Signal Processing*, 2013, pp. 5770–5774.

[9] Y. Huang, Y. Zhang, N. Li, Z. Wu, and J. A. Chambers, "A novel robust student's t-based kalman filter," *IEEE Transactions on Aerospace and Electronic Systems*, vol. 53, no. 3, pp. 1545–1554, 2017.

[10] Q. Li, Y. Ben, J. Tan, S. M. Naqvi, and J. Chambers, "Robust selection of the degrees of freedom in the student'st distribution through multiple model adaptive estimation," *Signal Processing*, vol. 153, pp. 255–265, 2018.

[11] Y. Huang, Y. Zhang, and J. A. Chambers, "A novel kullback–leibler divergence minimization-based adaptive student's t-filter," *IEEE Transactions on signal Processing*, vol. 67, no. 20, pp. 5417–5432, 2019.

[12] F. Tronarp, R. Hostettler, and S. Särkkä, "Sigma-point filtering for nonlinear systems with non-additive heavy-tailed noise," in *19th International Conference on Information Fusion*, 2016, pp. 1859–1866.

[13] S. Liu, K. Wang, and D. Abel, "Robust state and protection-level estimation within tightly coupled GNSS/INS navigation system," *GPS Solutions*, vol. 27, no. 3, p. 111, Apr. 20, 2023, ISSN: 1521-1886.

[14] J. Al Hage, P. Xu, and P. Bonnifait, "Student's t information filter with adaptive degree of freedom for multi-sensor fusion," in *22th International Conference on Information Fusion*, 2019, pp. 1–8.

[15] X. Bo and B. Shao, "Satellite selection algorithm for combined gps-galileo navigation receiver," in *2009 4th International Conference on Autonomous Robots and Agents*, IEEE, 2009, pp. 149–154.

[16] Z. Tao, P. Bonnifait, V. Frémont, J. Ibanez-Guzman, and S. Bonnet, "Road-centered map-aided localization for driverless cars using single-frequency GNSS receivers," *Journal of Field Robotics*, vol. 34, no. 5, pp. 1010–1033, 2017, ISSN: 1556-4967.

[17] S. Kotz and S. Nadarajah, *Multivariate t-distributions and their applications*. Cambridge University Press, 2004.

[18] H. Durrant-Whyte and T. C. Henderson, "Multisensor data fusion," in *Springer Handbook of Robotics*, 2008, pp. 585–610.

[19] M. Roth, T. Ardeshiri, E. Özkan, and F. Gustafsson, "Robust bayesian filtering and smoothing using student's t distribution," *arXiv preprint arXiv:1703.02428*, 2017.

[20] M. N. Do, "Fast approximation of kullback-leibler distance for dependence trees and hidden markov models," *IEEE signal processing letters*, vol. 10, no. 4, pp. 115–118, 2003.

[21] J. Al Hage, M. E. El Najjar, and D. Pomorski, "Multi-sensor fusion approach with fault detection and exclusion based on the kullback–leibler divergence: Application on collaborative multi-robot system," *Information Fusion*, vol. 37, pp. 61–76, 2017.

[22] P. Navarro Madrid, "Device and method for computing an error bound of a kalman filter based gnss position solution," pat., 2016.